Table 3
Intraindividual Standard Deviations (Sws) of FA and ADC Values of the Renal Cortex and Medulla Using Two ROIs (Upper Pole and Lower Pole) Within Right Kidney

	Location	FA								ADC (× 10^{-3} mm^2/s)							
		Cortex				Medulla				Cortex				Medulla			
		Mean	SD	(Sw)	%	Mean	SD	(Sw)	%	Mean	SD	(Sw)	%	Mean	SD	(Sw)	%
1	Upper	0.16	0.02			0.47	0.06			2.60	0.22			2.00	0.26		
	Lower	0.17	0.03	0.018	(10.7)	0.48	0.05	0.049	(10.4)	2.67	0.27	0.17	(6.4)	1.99	0.24	0.21	(10.5)
2	Upper	0.15	0.02			0.45	0.04			2.21	0.15			1.80	0.17		
	Lower	0.15	0.02	0.018	(12.2)	0.46	0.04	0.032	(7.2)	2.31	0.19	0.15	(6.6)	1.83	0.26	0.15	(8.0)
3	Upper	0.19	0.03			0.46	0.06			2.56	0.15			1.98	0.25		
	Lower	0.20	0.03	0.028	(14.4)	0.47	0.08	0.054	(11.5)	2.61	0.21	0.17	(6.4)	2.07	0.24	0.25	(12.2)
4	Upper	0.24	0.03			0.48	0.07			2.29	0.21			1.67	0.23		
	Lower	0.21	0.03	0.033	(18.0)	0.45	0.06	0.048	(11.1)	2.54	0.26	0.23	(8.6)	1.87	0.35	0.26	(11.7)
5	Upper	0.17	0.03			0.42	0.04			2.59	0.29			2.12	0.30		
	Lower	0.19	0.05	0.032	(14.2)	0.45	0.06	0.055	(11.9)	2.77	0.23	0.30	(12.2)	2.26	0.25	0.32	(17.8)

Values in parentheses are percentage values of of Sw followed by mean values.
FA, fractional anisotropy; ADC, apparent diffusion coefficient; Sw, intraindividual standard deviation based on two measurements from two ROIs (upper pole and lower pole) of the cortex/medulla of right kidney; SD, standard deviation of measurement of upper pole or lower pole ROI from data of 16 volunteers (interindividual standard deviation).

phragmatic motion helps to decrease misregistration (12). Unfortunately, this triggered acquisition technique could not be combined with DWI at the start of this study, owing to technical difficulties.

We used a minimum number of diffusion directions and a minimum number of b-values. Although a greater gradient orientation and measurement with more different b-values would result in more precise FA measurements, these changes will also increase acquisition time. In addition, recent reports have suggested that the difference among 6, 10, 15, and 30-orientation schemes in terms of the precision of the FA measurement is lower than test–retest reproducibility (13,14). Therefore, we believe that our choice of the six orientation schemes did not have a significant impact on our results.

Compared with the report by Ries et al (4), the average FA of the cortex in our study was slightly smaller, and that of the medulla was larger. Our ADC values were smaller than those of Ries et al for both the cortex and medulla. These differences might be explained by differences in MR protocols. Ries et al used pulse-triggering, which reduces the effect of pulsatile motion. Considering that the vessels in the medulla run parallel to the tubular structure, it is possible that medullary blood flow might result in a larger FA value in our study. The use of pulse triggering also affects ADC values, but Murtz et al (15) reported an increase in the ADC value when pulse-triggering was not used. Thus, the use of pulse triggering cannot explain this difference. We did not incorporate pulse triggering because dual (respiration and pulse) triggering requires a much longer acquisition time and is impractical. However, the SD in the repeated measurements increased when pulse-triggering was not used (15). Pulse triggering may be incorporated when imaging time is shortened by improving other techniques. It is of note that there were considerable variations in the FA/ADC values among the different sequences, especially for the cortical FA value. Previously reported ADC values of the renal cortex and

Table 4
Intraindividual Standard Deviations (Sws) of FA and ADC Values of the Renal Cortex and Medulla Using ROIs From Upper Pole of Right Kidney and Left Kidney

	Location	FA								ADC (× 10^{-3} mm^2/s)							
		Cortex				Medulla				Cortex				Medulla			
		Mean	SD	(Sw)	%	Mean	SD	(Sw)	%	Mean	SD	(Sw)	%	Mean	SD	(Sw)	%
1	Right	0.16	0.02			0.47	0.06			2.60	0.22			2.00	0.26		
	Left	0.19	0.03	0.025	(14.1)	0.45	0.05	0.034	(7.4)	2.61	0.17	0.17	(6.4)	2.04	0.17	0.24	(11.8)
2	Right	0.15	0.02			0.45	0.04			2.21	0.15			1.80	0.17		
	Left	0.16	0.02	0.024	(15.8)	0.44	0.05	0.029	(6.6)	2.30	0.16	0.12	(5.2)	1.86	0.11	0.13	(6.9)
3	Right	0.19	0.03			0.46	0.06			2.56	0.15			1.98	0.25		
	Left	0.21	0.03	0.029	(14.3)	0.45	0.06	0.055	(12.1)	2.59	0.22	0.17	(6.4)	2.08	0.32	0.17	(8.4)
4	Right	0.24	0.03			0.48	0.07			2.29	0.21			1.67	0.23		
	Left	0.21	0.04	0.036	(16.5)	0.42	0.05	0.062	(13.9)	2.54	0.25	0.24	(9.8)	2.02	0.27	0.34	(18.7)
5	Right	0.17	0.03			0.42	0.04			2.59	0.29			2.12	0.30		
	Left	0.24	0.03	0.062	(29.9)	0.44	0.05	0.033	(7.8)	2.55	0.24	0.20	(9.2)	2.12	0.22	0.22	(10.4)

Values in parentheses are percentage values of of Sw per mean values.
FA, fractional anisotropy; ADC, apparent diffusion coefficient; Sw, intraindividual standard deviation based on measurements of ROIs at right upper pole and left upper pole of the cortex /medulla; SD, standard deviation of measurement of ROIs at right upper pole or left upper pole of the cortex /medulla from data of 16 volunteers (interindividual standard deviation).

Table 5
Qualitative Evaluation of FA Maps and ADC Maps

Evaluation*	FA map					ADC map				
	3	4	5	Mean	SD	3	4	5	Mean	SD
1		4	12	4.8	0.4		3	13	4.8	0.4
2		1	15	4.9	0.3		3	13	4.8	0.4
3	3	12	1	3.9	0.5	1	9	6	4.3	0.6
4	2	6	8	4.4	0.7	2	8	6	4.3	0.7
5	15	1		3.1	0.4	4	8	4	4.0	0.7

*Evaluations were made in 5-grade scoring as follows: 1, not evaluable; 2, poor (cortex-medulla difference is not visible); 3, moderate (visible cortex-medulla difference, but not clear); 4, good (reasonable cortex-medulla difference); 5, excellent (clear cortex-medulla difference). No images included in the analysis were scored as 1 or 2.
FA, fractional anisotropy; ADC, apparent diffusion coefficient; SD, standard deviation of each measurement from data of 16 volunteers.

medulla measured by orthogonal DWI using single-shot EPI during breath-holding or free breathing are not consistent (3,5,6,16). Therefore, to use the ADC value as a marker of renal function, more standardized methods for measuring ADC are necessary.

Sequence 2 involved respiratory triggering with a higher b-value (400 s/mm^2) and consistently showed a lower FA/ADC value than sequence 1. The interindividual SD also tended to be lower than that in sequence 1. There has been no study examining FA value changes with different b-values using body DTI. In brain DTI, the FA value remains constant with different b-values (17). On the other hand, there is evidence that the ADC value decreases with a high b-value (1,17). ADC values with small maximum b-values (typically less than 100 s/mm^2) are affected by intravoxel coherent motion such as perfusion, and tend to be greater (15,18). In addition, interindividual SDs of ADC values are larger with smaller b-values (15,17,18). Initially, we started with a b-value of 200 s/mm^2 because we were concerned that the image with a b-value of 400 s/mm^2 resulted in a low signal owing to signal decay with higher b-values (17). However, our results suggest that the sequence with a b-value of 400 s/mm^2 seemed better in terms of accurate measurement and reflects diffusion, not perfusion.

Compared with baseline sequence 1, sequence 3 had a longer total acquisition time, slightly lower cortex–medulla contrast, and slightly larger intraindividual SD. Both sequences were virtually the same, except that 1) respiratory triggering was reset 10 times in sequence 3 and only 4 times in sequence 1; 2) the total number of averaging was 10 in sequence 3 compared with 12 (3 × 4) in sequence 1. Monitoring of respiration normally took 2–3 respirations (equivalent to 10–30 sec) before the actual triggered image acquisition started. Therefore, the different pretriggering monitoring processes in the six repeated sequences could explain the difference in total acquisition time, and consequently explain quite wide variations of measurements in sequence 3.

To identify the parameters for the optimal sequence, we used cortico-medullary differentiation on an FA map. Since the renal medulla is a radially oriented structure consisting of tubules, we expected differences in diffusion anisotropy. A previous article by Ries et al (4) also reported a higher anisotropy in the medulla. Therefore, we aimed at being able to differentiate between the cortex and medulla.

Ideally, SNR or contrast-to-noise ratio (CNR) should be measured. In our current analysis we used the parallel imaging technique to reduce the scanning time, thus modifying the background signal intensity. Therefore, SNR/CNR would not be an appropriate measurement (19). Moreover, owing to the FOV setting, there was no measurable air outside of the subject's body in some of the volunteers with large body size, which prevented us from determining the background signal intensity in these subjects. Image background seemed to be contaminated by artifacts from the moving intestines or aliasing artifacts in some images. An alternative method is to measure homogeneous regions close to the kidney (19) but homogeneous regions close to the kidney were hard to find. These factors made intersequential comparisons difficult. Instead, quality evaluation

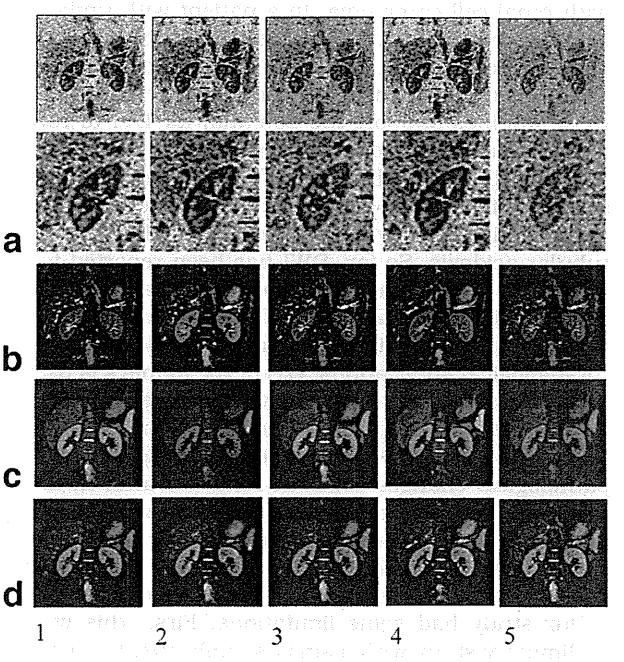

Figure 4. FA map (a), ADC map (b), b = 0 images (c), and diffusion-weighted images (d) obtained with different sequences in the same volunteer. Numbers 1–5 refer to the sequences in Table 1. The upper images of (a) are FA maps of the whole right kidney, and the lower images are the magnified views of the right kidney.

visually scored by radiologists was used. Based on the results of the cortex–medulla contrast and qualitative evaluation, sequences 1 and 2 offered the best protocol. The accurate quantification of FA/ADC is important in sequence optimization. We investigated this matter by measuring the Sw. Sequences 1 and 2 tended to show the lowest Sw in both ROIs within the right kidney and ROIs from the bilateral kidneys. However, the Sw was 12% of the mean FA value of the cortex and 7% of the mean FA value of the medulla in sequence 2. Other sequences showed Sw as high and as close to 30%. These results indicate the need for improving the accuracy of measurements before the quantification of FA/ADC is used in clinics and linked to pathology. Although we had limited data about reproducibility of FA/ADC measurement obtained in different dates, it is reassuring that the Sw in sequence 1 repeated on different dates did not differ considerably from the Sw obtained from the same examination (within the right kidney and from both kidneys).

We showed that the FA of the medulla was consistently higher than that of the cortex in all six sequences. This was considered to reflect the radially oriented architecture along the Henle loops, collecting tubules, and vascular bundles in the renal medulla. Since the renal medulla consists of tubular cells, and plays an important role in water transport, DTI provides a noninvasive tool to reveal renal pathological or physiological conditions with abnormal anisotropy and FA, and adds new information to isotropic diffusion-weighted imaging. Recently, Notohamiprodjo et al (8) applied DTI to 27 patients with various renal pathologies. Structural organization of the tumor (pseudocapsule or diffuse infiltration) was successfully detected in patients with renal cell carcinoma. In a patient with unilateral renal artery stenosis, an increase in FA and a decrease in ADC were seen. Although the exact underlying mechanism of these changes has not yet been explained, these findings support the potential for DTI to reveal pathological alterations in renal architecture. Other possible clinical applications of DTI include the evaluation and follow-up of diffuse renal diseases, especially for conditions involving the renal medulla, eg, renal tubular acidosis. So far, DWI has been reported to be useful for the evaluation of renal failure and in transplanted kidneys (1,2). Since DTI is proven to be as sensitive to changes in structural orientation as in neuroradiological applications, DTI of the kidneys is useful in evaluating conditions involving the renal medulla such as renal transplants, renal conditions after chemotherapy, or drug-induced renal damage, in which pathological changes occur in renal tubules. In addition, with further improvements in spatial resolution DTI of the kidneys offers the potential for noninvasive visualization of underlying structural changes, as shown in the above example of renal cell carcinoma.

Our study had some limitations. First, this was a preliminary study with a small sample size. It is necessary to optimize the protocols, reproducibility, and repeatability of FA values and ADC values. Second, this study was performed with healthy volunteers of a relatively young age. Therefore, the results may be different in older patients, who might have difficulties in respiratory triggering. In respiratory gating, the acquisition time increases when patients have an irregular rhythm or depth of breathing. An average examination time of less than 7 minutes per sequence is clinically acceptable. However, the examination time might take longer than that in the clinics. To shorten the image acquisition time and decrease misregistration, the use of navigator-triggered acquisition, as discussed above, might be a solution. Third, the absence of a pulse trigger, as mentioned previously, might be another limitation. For some respiratory-triggered sequences (ie, sequences 1, 2, and 4) the number of signal averaging multiplied by the series number was 12, which was larger than the 10 averages in other series. This slight difference might explain the differences in image quality. Another concern is the effects of artifacts. Despite efforts to prevent artifacts, various types of artifacts such as aliasing artifacts, N-half artifacts, susceptibility artifacts, and ghost artifacts can be observed in echo-planer imaging. We did not evaluate them because it would have been difficult to quantify the effects of these artifacts on image quality, but their possible effects should be considered. Finally, SNR measurement was not included in the analysis, as explained above. Qualitative evaluation scored visually may be used as an alternative marked of image quality.

In conclusion, our preliminary study demonstrated that DTI of the kidneys with respiratory-triggered acquisition was feasible. Among five different sequences, a 3-mm slice thickness, three signal averages, and a b-value of 200 or 400 s/mm^2 resulted in excellent cortex–medulla contrast on FA maps with smaller intraindividual variations with better image quality.

ACKNOWLEDGMENTS

The authors thank Dr. Osamu Takizawa and Chiaki Imura (Siemens-asahi Medical Technologies Ltd.) for excellent technical assistance and advice for sequence optimization; Dr. Yukio Miki and Yasutaka Fushimi (Department of Diagnostic Imaging and Nuclear Medicine, Kyoto University) for professional advice on 3 T sequences; Akira Hiraga (Department of Radiology, Kyoto University) for technical support; and all the volunteers who were willing to participate in the study.

REFERENCES

1. Thoeny HC, De Keyzer F, Oyen RH, Peeters RR. Diffusion-weighted MR imaging of kidneys in healthy volunteers and patients with parenchymal diseases: initial experience. Radiology 2005:235:911–917.
2. Vermathen P, Zumstein D, Eisenberger U, et al. Functional MRI of transplanted human kidneys evaluated by diffusion-weighted MRI—initial experience. In: Proc 13th Annual Meeting ISMRM, Miami, 2005. Abstract 556.
3. Muller MF, Prasad PV, Bimmler D, Kaiser A, Edelman RR. Functional imaging of the kidney by means of measurement of the apparent diffusion coefficient. Radiology 1994:193:711–715.
4. Ries M, Jones RA, Basseau F, Moonen CT, Grenier N. Diffusion tensor MRI of the human kidney. J Magn Reson Imaging 2001:14: 42–49.
5. Siegel CL, Aisen AM, Ellis JH, Londy F, Chenevert TL. Feasibility of MR diffusion studies in the kidney. J Magn Reson Imaging 1995:5: 617–620.

6. Fukuda Y, Ohashi I, Hanafusa K, et al. Anisotropic diffusion in kidney: apparent diffusion coefficient measurements for clinical use. J Magn Reson Imaging 2000:11:156–160.
7. Basser PJ, Pierpaoli C. Microstructural and physiological features of tissues elucidated by quantitative-diffusion-tensor MRI. J Magn Reson B 1996:111:209–219.
8. Notohamiprodjo M, Glaser C, Herrmann A, et al. MR diffusion tensor imaging of the kidney with parallel imaging – initial clinical experience. In: Proc 15th Annual Meeting ISMRM, Toronto, 2007. Abstract 3686.
9. Griswold MA, Jakob PM, Heidemann RM, et al. Generalized autocalibrating partially parallel acquisitions (GRAPPA). Magn Reson Med 2002:47:1202–1210.
10. Bland JM, Altman DG. Measurement error. BMJ 1996:313:744.
11. Taouli B, Martin AJ, Qayyum A, et al. Parallel imaging and diffusion tensor imaging for diffusion-weighted MRI of the liver: preliminary experience in healthy volunteers. AJR Am J Roentgenol 2004: 183:677–680.
12. Klessen C, Asbach P, Kroencke TJ, et al. Magnetic resonance imaging of the upper abdomen using a free-breathing T2-weighted turbo spin echo sequence with navigator triggered prospective acquisition correction. J Magn Reson Imaging 2005:21:576–582.
13. Farrell JA, Landman BA, Jones CK, et al. Effects of signal-to-noise ratio on the accuracy and reproducibility of diffusion tensor imaging-derived fractional anisotropy, mean diffusivity, and principal eigenvector measurements at 1.5 T. J Magn Reson Imaging 2007: 26:756–767.
14. Landman BA, Farrell JA, Jones CK, Smith SA, Prince JL, Mori S. Effects of diffusion weighting schemes on the reproducibility of DTI-derived fractional anisotropy, mean diffusivity, and principal eigenvector measurements at 1.5T. Neuroimage 2007:36:1123–1138.
15. Murtz P, Flacke S, Traber F, van den Brink JS, Gieseke J, Schild HH. Abdomen: diffusion-weighted MR imaging with pulse-triggered single-shot sequences. Radiology 2002:224:258–264.
16. Namimoto T, Yamashita Y, Mitsuzaki K, Nakayama Y, Tang Y, Takahashi M. Measurement of the apparent diffusion coefficient in diffuse renal disease by diffusion-weighted echo-planar MR imaging. J Magn Reson Imaging 1999:9:832–837.
17. Melhem ER, Itoh R, Jones L, Barker PB. Diffusion tensor MR imaging of the brain: effect of diffusion weighting on trace and anisotropy measurements. AJNR Am J Neuroradiol 2000:21:1813–1820.
18. Kim T, Murakami T, Takahashi S, Hori M, Tsuda K, Nakamura H. Diffusion-weighted single-shot echoplanar MR imaging for liver disease. AJR Am J Roentgenol 1999:173:393–398.
19. Heverhagen JT. Noise measurement and estimation in MR imaging experiments. Radiology 2007:245:638–639.

ELSEVIER

European Journal of Radiology 71 (2009) 486–491

EJR
EUROPEAN JOURNAL OF RADIOLOGY

www.elsevier.com/locate/ejrad

Whole-heart coronary magnetic resonance angiography with parallel imaging: Comparison of acceleration in one-dimension vs. two-dimensions

Tomohisa Okada[a,*], Shotaro Kanao[a], Ayako Ninomiya[b], Saori Sato[b], Shigehide Kuhara[b], Toshikazu Kamae[a], Kimio Gotoh[a], Kaori Togashi[a]

[a] *Department of Diagnostic Radiology, Kyoto University, 54 Shogoin Kawaharacho, Sakyoku, Kyoto 606-8507, Japan*
[b] *Toshiba Medical Systems Corporation, Otawara-shi, Tochigi 324-8550, Japan*

Received 24 January 2008; received in revised form 17 May 2008; accepted 3 June 2008

Abstract

Purpose: To evaluate visualization of the whole-heart coronary arteries accelerated with parallel imaging (PI) applied in two-dimension (2D) in comparison with one-dimension (1D).

Materials and methods: Seventeen healthy subjects were studied with a 1.5-T scanner equipped with a whole body phased array coil system and 16-channel receivers. Using 16 coil elements, whole-heart coronary magnetic resonance angiography (CMRA) was acquired in two conditions of 1D-PI and 2D-PI. The former scan was accelerated in phase direction by factor of 2 and the latter in phase and slice directions by factors of 2.5 and 2, respectively. Visualized length of right coronary artery (RCA), left anterior descending artery (LAD), and left circumflex artery (LCX) was measured. Signal-to-noise ratio (SNR) and contrast-to-noise ratio (CNR) was also measured. The CMRA quality was assessed in segment-wise with a five-point scale.

Results: The average scan time decreased to 5.3 ± 2.2 min in 2D-PI from 11.6 ± 3.5 min in 1D-PI, reducing the scan time to 45%. The visualized length, SNR, and CNR in average were smaller for images of 2D-PI compared with those of 1D-PI, however, statistically significant results were observed only in RCA ($P < 0.05$). Score reduction of 2D-PI image quality was limited to 0.34 in average, and only two out of fifteen segments (#2, 6) showed significant score deterioration ($P < 0.05$).

Conclusions: Compared with the relatively limited degree of image degradation, 2D-PI offered a large reduction of the acquisition time, which is of large benefit in clinical situations.

Keywords: Coronary magnetic resonance angiography; Parallel imaging; Whole-heart

1. Introduction

Coronary magnetic resonance angiography (CMRA) does not require the use of ionizing radiation and has been proven to be of clinical value to detect the coronary artery disease non-invasively [1]. However, routine clinical CMRA remains challenging due to small vessel size, tortuosity, obscuring signal form fat and myocardium, physiological motion, and long scan time, as long as 13.8 min in average for the whole heart [2]. The use of parallel imaging techniques [3] has enabled CMRA acquisition to be accelerated by factors of 2–3 [2,4]. The reduction in imaging time allowed whole heart coverage.

Many of the former scan time reduction, however, was attained with parallel imaging used only in one dimension, usually in the phase encoding direction. Further reduction in scan time has been reported by applying the parallel method in two dimensions [5,6] and recent inventions of multi-array coils allow usage of this mode. The new scan method will reduce the acquisition time but deteriorate the image quality at the same time. The optimal coil setup and parallel acceleration factors for speeding in two directions was investigated in terms of signal-to-noise ratio (SNR) [7]. A coil system dedicated to CMRA is not always available, however, recent trend to cover the whole body allows us to use a phased-array coil that consists of more than 10 coils

* Corresponding author. Tel.: +81 75 751 4215; fax: +81 75 751 4216.
E-mail address: tomokada@kuhp.kyoto-u.ac.jp (T. Okada).

0720-048X/$ – see front matter © 2008 Elsevier Ireland Ltd. All rights reserved.
doi:10.1016/j.ejrad.2008.06.005

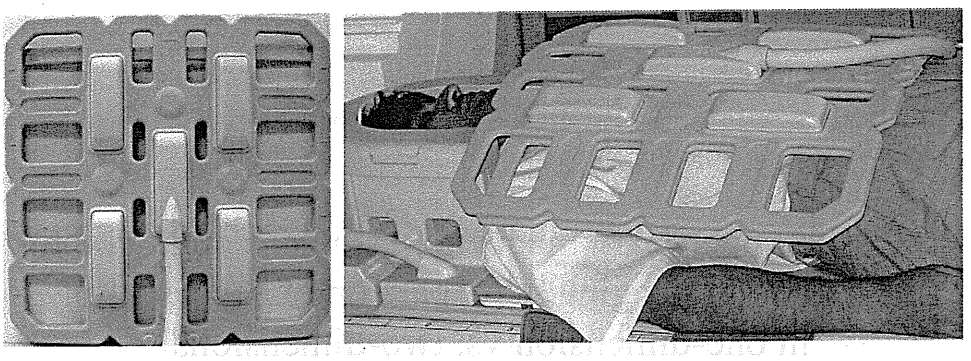

Fig. 1. The coil design and setup. Images of the front coil viewed from the top (left) and placed around a subject (right). The width is 55 cm and length is 50 cm. The coil elements are arranged in four by four. A pair of two transverse coil element rows was used for the acquisition. The back coil has the same geometry without flexibility.

at a time. Such a multi-array body coil system has gradually become clinically available and would enable parallel imaging in two dimensions.

Hence, in this study we hypothesized that a multi-array coil system to cover wide area of the body can also be used for faster coronary imaging operated in two-dimensional (2D) parallel imaging (PI) mode with acceptable image quality compared with coronary images acquired in one-dimensional (1D) PI mode.

2. Materials and methods

2.1. Subjects

Seventeen healthy volunteers (thirteen males and four females, mean age: 23 ± 3 years) without previous history of diseases were enrolled in this study, after obtaining written informed consents. The study was approved by the Institutional Committee on Human Research.

2.2. Imaging protocol

The study was performed with a 1.5-T MR system (Vantage powered by Atlas, Toshiba Medical Systems, Otawara-shi, Japan) equipped with a pair of 4 by 4 phased array coils placed at both front and back of the chest (Fig. 1). Two top rows were used for both front and back coils, resulting in 16 active coil elements connected to 16 receiver channels.

A localizing scan was performed to locate the heart and the diaphragm in three orthogonal stacks, as well as to confirm adequate coil position, followed by a reference scan to determine the individual coil sensitivities for subsequent parallel scans [3,5]. After acquiring T1-weighted heart images in coronal, axial and parasagittal planes, cine images were scanned in four-chamber view using SSFP sequence (repetition time (TR) 4.3 ms, echo time (TE) 2.2 ms, flip angle (FA) 120°) for 50–60 frames/heart beat. On these images, the interval of minimal right coronary artery (RCA) motion was visually assessed, and acquisition windows for all subsequent scans were planned to fall within that period of minimal RCA motion [4]. Respiratory motion during the acquisition of the coronary scans was compensated for by using prospective real-time triggering (triggering window 4.65 mm) and volume tracking (motion correction factor 0.6) based on the one-dimensional data of the right diaphragm position [8]. For cardiac synchronization and monitoring, two electrodes were placed on the left anterior hemithorax of the subject and the R wave of the electrocardiogram used as a trigger for image acquisition.

For the whole-heart coronary scan, magnetization was prepared by a T2-preparation pulse, followed by a frequency-selective fat saturation pulse and a spoiler gradient [9]. Three-dimensional (3D), centric-ordered, segmented, refocused SSFP sequence (TR 4.3 ms, TE 2.2 ms, FA 120°) was used to cover the entire heart in 70–80 transverse slices of 1.5 mm thickness, with an in-plane readout and phase encodings of 256×168 resulting in resolution of 1.3 mm and 1.5–1.9 mm, respectively dependent on the size of the subjects. The image was reconstructed to the voxel size of $0.6\,\text{mm} \times 0.6\,\text{mm} \times 0.75\,\text{mm}$. An automated shim procedure was applied to the area covering the heart. The subjects were scanned with both 1D-PI and 2D-PI. Acceleration was applied in phase-encoding direction with the factor of 2 for 1D-PI and in both phase- and slice-encoding directions with the factors of 2.5 and 2, respectively, for 2D-PI. The acquisition window was segmented into 4 and 3 for 1D-PI and 2D-PI, respectively. The order of the two parallel scans was randomized.

2.3. Image processing and measurements

The data of 3D CMRA was transferred to a commercially available workstation with image reconstruction software (AZE Virtual Place, AZE Ltd., Tokyo, Japan). For each of the RCA, left anterior descending (LAD), and left circumflex (LCX), multiple contiguous sections were selected and curved planar reconstruction (CPR) was conducted by a radiological technologist. The order of subject data processing and evaluation was made blind to the radiologists. Left main trunk was treated as a part of LAD. The length of visualized RCA, LAD, and LCX was measured. Signal-to-noise ratio (SNR) and contrast-to-noise ratio (CNR) was also measured at 1 cm distal to RCA and LCA by placing a region-of-interest (ROI) at the arteries and the background beside them [10]. The mean blood signal intensity at the coronary artery (SI_{blood}) and its standard deviation (SD_{blood}) were

calculated and the SNR was defined as SI_{blood}/SD_{blood}. Contrast between coronary blood and background was calculated using mean signal intensity of background ($SI_{background}$) and its standard deviation ($SD_{background}$) as [9,10]:

$$CNR = \frac{(SI_{blood} - SI_{background})/(SD_{blood} + SD_{background})}{2} \quad (1)$$

2.4. Assessment of image quality

Assessment of 3D CMRA was conducted on segment-wise classified by the American Heart Association: RCA was divided into segments 1–4, LAD was divided into segments 5–10, and LCX was divided into segments 11–15 by two readers (T.O. and S.K.) in consensus. In order to grade the image quality of all the coronary artery segments, a five-point grading system was used: (4) excellent (the vessel was well depicted with sharply defined borders), (3) fair (the vessel was adequately visualized, with confidence in the diagnosis, only mildly blurred borders), (2) good (coronary was visible, but confidence in the diagnosis was low, due to moderately blurred borders), (1) poor (coronary vessel barely seen, or was obscured by noise), and (0) not visualized [2,11]. For the evaluation, both the original and CPR images were used. All values are presented as the mean plus or minus standard deviation (mean ± S.D.).

2.5. Statistical analysis

Comparisons were made by means of paired *t*-test for continuous variables and Mann–Whitney test for nominal variables. In all cases, a two-tailed test was performed. *P* values of 0.05 or less were considered statistically significant after correction of multiple comparisons for each item evaluated.

3. Results

3.1. Subject characteristics

The average heart rate of the subjects was 56 beats per min (BPM), ranged form 43 to 70 BPM, and the acquisition was performed at stationary period in diastolic phase [11]. The mean stationary period of RCA was 206 ms, varied from 80 to 400 ms. The length of acquisition window for each TR period was 98.7 ms for 1D-PI and 107.3 ms for 2D-PI. Only one subject with a heart rate of 65 BPM had the stationary period 80 ms, which was less than the length of the acquisition windows. The 1D-PI took 11.6 ± 3.5 min and 2D-PI took 5.3 ± 2.2 min in average ± S.D., reducing the scan time to 45%.

3.2. Visualized length, SNR and CNR

The visualized lengths in average were 125.3 ± 17.6 mm and 113.5 ± 20.1 mm for RCA, 119.6 ± 21.4 mm and 113.1 ± 21.2 mm for LAD, and 81.3 ± 25.0 and 75.0 ± 18.8 mm for LCX, respectively, for 1D-PI and 2D-PI (Fig. 2). All the arteries were visualized longer in 1D-PI, but the differences were significant only in RCA ($P < 0.05$).

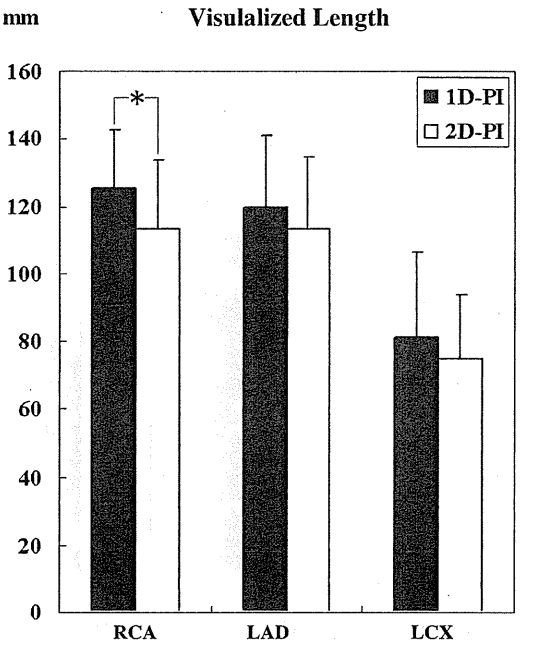

Fig. 2. Visualized length of RCA, LAD, and LCX. All arteries visualized were shorter in images acquired in 2D-parallel mode in comparison with those acquired in 1D mode. The differences were significant only in RCA (*$P < 0.05$). RCA: right coronary artery, LAD: left anterior descending artery, LCX: left circumflex artery.

Mean ROI areas (mm^2) were 45.6 ± 10.0 and 45.1 ± 10.3 at RCA, and 43.9 ± 9.1 and 42.5 ± 8.4 at LCA, respectively, for artery and background. Mean SNR was 7.4 ± 3.2 and 6.0 ± 2.6 for RCA, and 5.8 ± 1.8 and 5.5 ± 1.4 for LCA, and CNR were 7.8 ± 2.7 and 6.2 ± 1.7 for RCA, and 6.8 ± 2.3 and 6.2 ± 1.9 for LCA, respectively, for 1D-PI and 2D-PI (Fig. 3). Statistically significant results were observed only in RCA when images of 1D-PI and 2D-PI were compared in terms of both SNR, and CNR ($P < 0.05$).

3.3. Image quality evaluation

The score reduction was limited to 0.34 in average and only three segments (#2, 3, 14) deteriorated by more than 0.5 point (0.53–0.65) when the images acquired in 2D-PI were compared with those acquired in 1D-PI (Table 1). Although two segments (#2, 6) showed statistically significant deterioration for the 2D-parallel scan ($P < 0.05$), differences in scores were relatively small and coronary images were comparable (Fig. 4). In one case, apparent unfolding error was observed in 2D mode but it did not affect the evaluation.

4. Discussions

For widely available RF coils with a few arrays, the noise amplifies rapidly as the acceleration factor increases and current accelerations in clinical use are generally up to 2–3. Although unacceptable degeneration of SNR is inevitable at high 1D acceleration due to steep increase of the g-factor, use of multiple RF

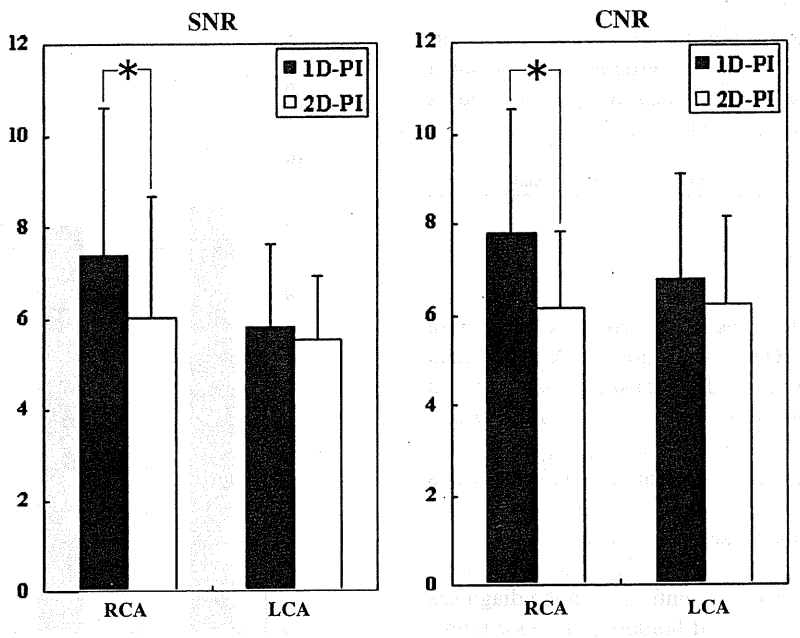

Fig. 3. SNR and CNR at proximal regions of RCA and LCA. Images acquired in 2D-parallel mode showed lower SNR and CNR in average when compared with those acquired in 1D mode. The differences were significant only in RCA (*$P < 0.05$). SNR: signal-to-noise ratio, CNR: contrast-to-noise ratio, RCA: right coronary artery, LCA: left coronary artery.

coils arranged in two dimensions can alleviate noise amplification [12]. Parallel imaging applied simultaneously to the phase- and slice-encoding directions in 3D acquisition can diminish deterioration of SNR caused by acceleration [5,6]. Hence, application of multidimensional RF coil arrays can extend the capabilities of CMRA by alleviating the SNR penalty from scan acceleration. The whole-heart CMRA scans a thick slab that spans multiple coil elements, and brings parallel imaging in the slice direction into practical use. Larger scan volume has also the advantage of offsetting SNR losses from acceleration through 3D noise averaging [13]. This kind of volume acquisition with high acceleration factors using parallel imaging was enabled by recent introduction of phased array coil systems that covers large part of the body. This study illustrated attainable advantage of this type of coil system applied for CMRA.

Table 1
Image quality scores of coronary artery segments in the 1D- and 2D-parallel scans

Coronary artery segment	Image quality scores (mean ± S.D.)		Difference[a]
	1D-parallel scan	2D-parallel scan	
#1	3.8 ± 0.56	3.5 ± 0.62	0.24
#2	3.4 ± 1.0	2.8 ± 0.90[b]	0.65[c]
#3	2.4 ± 1.3	1.9 ± 1.1	0.53[c]
#4	0.94 ± 1.0	0.71 ± 0.85	0.24
#5	3.6 ± 0.49	3.4 ± 0.70	0.29
#6	3.3 ± 0.69	2.8 ± 0.95[b]	0.47
#7	3.0 ± 0.61	2.8 ± 0.73	0.18
#8	2.0 ± 0.71	1.6 ± 0.79	0.35
#9	2.1 ± 0.99	1.9 ± 0.97	0.18
#10	0.82 ± 0.88	0.59 ± 0.94	0.24
#11	3.3 ± 0.77	3.0 ± 0.94	0.29
#12	1.7 ± 1.4	1.2 ± 1.1	0.47
#13	2.4 ± 0.86	2.1 ± 0.90	0.29
#14	1.6 ± 1.1	1.0 ± 1.1	0.65[c]
#15	0.18 ± 0.53	0.18 ± 0.53	0

[a] Differences show the amount of score reduction in 2D- from 1D-parallel scan.
[b] Segments with significant score reduction in 2D-parallel scan ($P < 0.05$).
[c] Segments with score reduction by more than 0.5 in 2D-parallel scan.

In the quantitative analysis of visualized length, SNR, and CNR, all the three coronary arteries were visualized better in 1D-PI compared with 2D-PI. However, the statistical analysis showed significant differences in the RCA only. Much of the differences may attribute to the SNR reduction intrinsic to the parallel imaging, but physiological noise also has to be taken into accounted. The duration of the cardiac rest period was reported to be shorter for the RCA compared to the LAD and the onset of the rest period was more delayed for the RCA in the averaged data of 15 subjects [14]. In a CMRA study of 210 consecutive patients, however, Jahnke et al. observed that in about one-third of patients, rest period of LCA began later or was shorter than that of RCA [15]. The translational motion of the RCA is approximately twice that of the LCA [16]. Moreover, the assessment of coronary motion in a single imaging plane is limited because the 3D movement of the vessels – in particular, motion through the imaging plane and the motion at different levels of the vessel – cannot be completely assessed [16]. In this study, estimation of coronary rest period was visually assessed on the RCA in a single plane. Undetected motion of LCA might result in slight increase of motion artifact, which was observed as decreased visualized length, SNR, and CNR.

In terms of the qualitative analysis, degradation of coronary visualization was limited in many of the segments in 2D-parallel scan images in comparison with those acquired in 1D mode. The

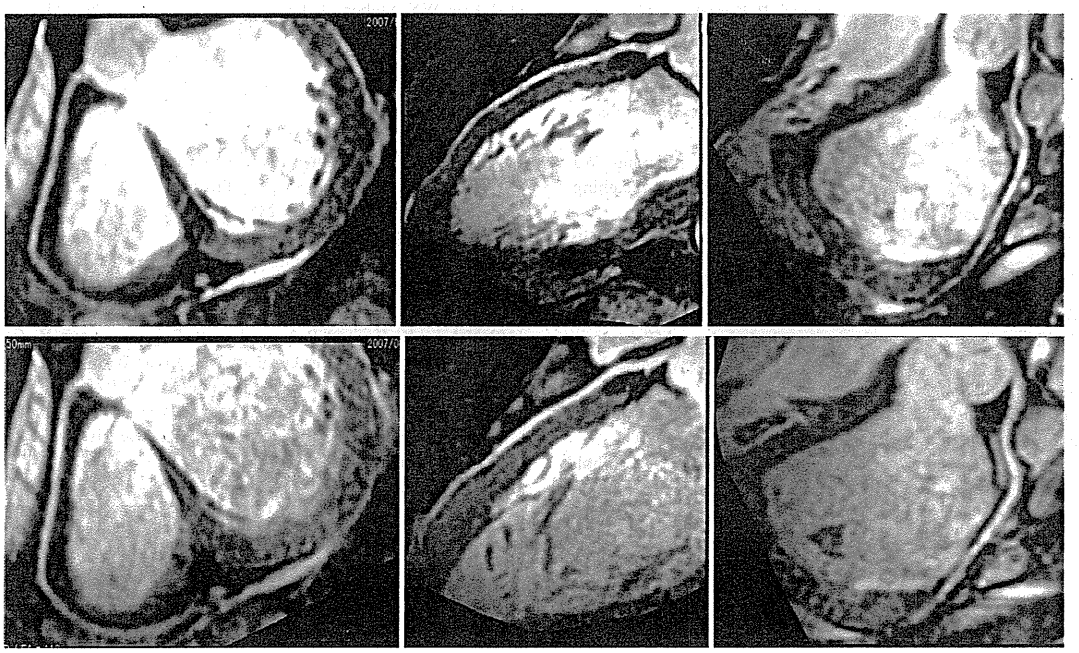

Fig. 4. Representative coronary MRA images acquired in 1D- and 2D-parellel acceleration. Images of RCA (left), LAD (middle), and LCX (right) acquired in 1D-parallel mode (factors: 2 × 1) are presented on the upper row and images acquired in 2D-parallel mode (factors: 2.5 × 2) are on the lower row. Excellent quality images were obtained in 2D-parallel mode comparable to those in 1D mode. The abbreviations are the same as in Fig. 2.

score reduction was 0.34 in average and it may not result in a significant problem for making a diagnosis. The parallel imaging factors in this study is almost the maximum available in the current setup. It should be noted that the RF coil array used in this study was optimized for the body, not for the heart. In one case, apparent unfolding error was observed in 2D-parallel acquisition. It probably resulted from the fact that only two rows of coil arrays were used to cover the whole heart and separation of signals in slice direction was not complete. The parallel imaging factor might be reduced in some case, especially in the slice encoding direction. Appreciable improvement in visualization would be attained through further reductions in the coil size and increases in the density of the array elements, such as a 32-channel coil array [13,17,18], which is out of the current focus.

In this study, we scanned normal volunteers, which is a limitation of this study and the results of this study have to be validated in clinical population and compared with reference standard such as coronary angiography. Despite the necessity for further investigation, the results of normal volunteers are significant when we consider the wide-spread usage of multi-detector CT coronary angiography. Seventy-five percent of patient with acute chest pain had no significant CT findings and a final diagnosis of clinically insignificant chest pain in a study [19]. The number of application of CT coronary angiography to patients with acute chest pain will increase in the near future. It may save some more patients at risk but increase exposure to radiation and contrast materials. The risk of carcinogenesis caused by diagnostic X-rays, especially CT is not negligible [20]. The whole-heart acquisition in around 5 min may open a new window to wider use of CMRA such as a screening purpose, although further clinical validations have to be provided.

5. Conclusion

In the present study, capability of more rapid coronary imaging was illustrated by using 2D-parallel acquisition mode. Although there was deterioration of the image quality, the extent was limited and may contribute to wider employment of coronary MR angiography.

Acknowledgement

This study was conducted as a part of the project, "R&D of Molecular Imaging Equipment for Malignant Tumor Therapy Support," supported by NEDO (New Energy and Industrial Technology Development Organization), Japan.

References

[1] Kim WY, Danias PG, Stuber M, et al. Coronary magnetic resonance angiography for the detection of coronary stenoses. N Engl J Med 2001;345:1863–9.
[2] Sakuma H, Ichikawa Y, Suzawa N, et al. Assessment of coronary arteries with total study time of less than 30 min by using whole-heart coronary MR angiography. Radiology 2005;237:316–21.
[3] Pruessmann KP, Weiger M, Scheidegger MB, Boesiger P. SENSE: sensitivity encoding for fast MRI. Magn Reson Med 1999;42:952–62.
[4] Weber OM, Martin AJ, Higgins CB. Whole-heart steady-state free precession coronary artery magnetic resonance angiography. Magn Reson Med 2003;50:1223–8.
[5] Weiger M, Pruessmann KP, Boesiger P. 2D SENSE for faster 3D MRI. Magma 2002;14:10–9.
[6] Ohliger MA, Grant AK, Sodickson DK. Ultimate intrinsic signal-to-noise ratio for parallel MRI: electromagnetic field considerations. Magn Reson Med 2003;50:1018–30.

[7] Buehrer M, Huber ME, Wiesinger F, Boesiger P, Kozerke S. Coil setup optimization for 2D-SENSE whole-heart coronary imaging. Magn Reson Med 2006;55:460–4.
[8] Danias PG, McConnell MV, Khasgiwala VC, Chuang ML, Edelman RR, Manning WJ. Prospective navigator correction of image position for coronary MR angiography. Radiology 1997;203:733–6.
[9] Botnar RM, Stuber M, Danias PG, Kissinger KV, Manning WJ. Improved coronary artery definition with T2-weighted, free-breathing, three-dimensional coronary MRA. Circulation 1999;99:3139–48.
[10] Dirksen MS, Lamb HJ, van der Geest R, de Roos A. Toward comparability of coronary magnetic resonance angiography: proposal for a standardized quantitative assessment. Eur Radiol 2003;13:2353–7.
[11] Wu YW, Tadamura E, Yamamuro M, Kanao S, Nakayama K, Togashi K. Evaluation of three-dimensional navigator-gated whole heart MR coronary angiography: the importance of systolic imaging in subjects with high heart rates. Eur J Radiol 2007;61:91–6.
[12] Wiesinger F, Boesiger P, Pruessmann KP. Electrodynamics and ultimate SNR in parallel MR imaging. Magn Reson Med 2004;52:376–90.
[13] Niendorf T, Hardy CJ, Giaquinto RO, et al. Toward single breath-hold whole-heart coverage coronary MRA using highly accelerated parallel imaging with a 32-channel MR system. Magn Reson Med 2006;56:167–76.
[14] Kim WY, Stuber M, Kissinger KV, Andersen NT, Manning WJ, Botnar RM. Impact of bulk cardiac motion on right coronary MR angiography and vessel wall imaging. J Magn Reson Imaging 2001;14:383–90.
[15] Jahnke C, Paetsch I, Achenbach S, et al. Coronary MR imaging: breath-hold capability and patterns, coronary artery rest periods, and beta-blocker use. Radiology 2006;239:71–8.
[16] Hofman MB, Wickline SA, Lorenz CH. Quantification of in-plane motion of the coronary arteries during the cardiac cycle: implications for acquisition window duration for MR flow quantification. J Magn Reson Imaging 1998;8:568–76.
[17] Hardy CJ, Cline HE, Giaquinto RO, Niendorf T, Grant AK, Sodickson DK. 32-element receiver-coil array for cardiac imaging. Magn Reson Med 2006;55:1142–9.
[18] Nehrke K, Bornert P, Mazurkewitz P, Winkelmann R, Grasslin I. Free-breathing whole-heart coronary MR angiography on a clinical scanner in four minutes. J Magn Reson Imaging 2006;23:752–6.
[19] White CS, Kuo D, Kelemen M, et al. Chest pain evaluation in the emergency department: can MDCT provide a comprehensive evaluation? AJR Am J Roentgenol 2005;185:533–40.
[20] Berrington de Gonzalez A, Darby S. Risk of cancer from diagnostic X-rays: estimates for the UK and 14 other countries. Lancet 2004;363:345–51.

Int J Cardiovasc Imaging (2009) 25:397–403
DOI 10.1007/s10554-008-9398-x

ORIGINAL PAPER

Facilitated acquisition of whole-heart coronary magnetic resonance angiography with visual feedback of respiration status

Tomohisa Okada · Shigehide Kuhara · Shotaro Kanao · Ayako Ninomiya · Saori Sato · Toshikazu Kamae · Kimio Gotoh · Kaori Togashi

Received: 26 May 2008 / Accepted: 1 December 2008 / Published online: 16 December 2008

Abstract Three dimensional (3D) whole-heart (WH) coronary MR angiography (CMRA) requires an extended imaging time, but it may be reduced by providing a subject with visual feedback (VFB). Thirteen healthy volunteers were scanned and quality of 3D WH-CMRA images was compared among three scan conditions: free breathing (FB) with and without VFB (FB + VFB and FB − VFB, respectively) and multiple breath-holds with VFB (MBH + VFB). All but two subjects were able to complete all scans. The average scan times were 10.0 ± 2.2, 10.0 ± 2.5, and 8.2 ± 1.3 min for FB − VFB, FB + VFB, and MBH + VFB, respectively. In the MBH + VFB condition, scan time was significantly reduced by 18% compared with both FB scans. No significant difference in image quality was observed between the FB − VFB and MBH + VFB conditions, but scores were significantly deteriorated at some segments in the FB + VFB condition. The MBH + VFB scan can be performed with a shorter scan time without failure or impairment of image quality.

Keywords Coronary artery · Whole-heart · Visual feedback · Breath-hold · Free-breathing

T. Okada (✉) · S. Kanao · T. Kamae · K. Gotoh · K. Togashi
Department of Diagnostic Radiology, Kyoto University Graduate School of Medicine, 54 Shogoin Kawaharacho, Sakyoku, Kyoto 606-8507, Japan
e-mail: tomokada@kuhp.kyoto-u.ac.jp

S. Kuhara · A. Ninomiya · S. Sato
Toshiba Medical Systems Corporation, Otawara-shi, Tochigi 324-8550, Japan

Introduction

High resolution MRI image is required to observe detailed anatomical features and abnormalities of the coronary artery, which facilitates acquisition in three-dimensional (3D) mode. Furthermore, it allows a simpler imaging setup even for the tortuous coronary artery and generates thin contiguous slices, which minimize partial volume effects and is suitable for post-processing [1, 2]. Most 3D whole-heart (WH) coronary MR angiography (CMRA) studies are performed during free breathing while monitoring the diaphragm position, which has three main limitations [3]: rejection of acquired data, more effect of respiratory motion [4, 5] and change in breathing pattern that results in image blurring [5, 6]. These problems can be attributed to the fact that patients cannot recognize their breathing level and therefore cannot adjust it.

Respiratory motion is principally in the superior-inferior direction with a range exceeding 10 mm [7]. In order to facilitate patients to cope with such a large respiratory motion for CMRA, a system for feedback

of diaphragm position was proposed [8]. The feedback system has been effective in single-slice acquisition [3], and applied to 3D acquisition covering a limited volume in multiple breath-holds [9]. Imaging strategies of CMRA have tended to focus on the use of a single method of either breath-holding or free-breathing for all patients, however, significant variations exist among patients in terms of breath-holding ability and respiratory regularity that make the use of a single technique alone unlikely to be universally successful [10]. Therefore, giving a subject options for respiration control may allow for better results.

Hence, this study was conducted to investigate the effectiveness of a visual feedback (VFB) system of diaphragm position in the WH-CMRA scan in either multiple breath-holding or free-breathing VFB conditions. The scan time and image quality were evaluated in comparison with free-breathing scan without VFB (i.e. a conventional scan method) as a reference standard.

Methods

Subjects

After obtaining written informed consent, 13 healthy volunteers (eight males and five females, age 20–44, mean 25 years of age) without previous history of diseases were enrolled in this study. The study was approved by the Institutional Committee on Human Research.

Imaging protocol

The study was performed with a 1.5-T MR system (Vantage powered by Atlas, Toshiba Medical Systems, Otawara-shi, Japan) equipped with a pair of 4 by 4 phased array coils placed at both the front and back of the chest. Two top rows were used for both front and back coils, resulting in 16 active coil elements connected to 16 receiver channels.

A localizing scan was performed to locate the heart and the diaphragm in three orthogonal stacks, as well as to confirm adequate coil position, followed by a reference scan to determine the individual coil sensitivities for subsequent parallel imaging [11, 12]. Cine images were acquired in 4-chamber view using steady-state free precession (SSFP) sequence [repetition time (TR) 4.3 ms, echo time (TE) 2.2 ms, flip angle (FA) 120°] for 50–60 frames/heart beat. The interval of minimal right coronary artery (RCA) motion was visually assessed and acquisition windows for all subsequent scans were planned to fall within the rest period of RCA motion [13].

For the whole-heart coronary scan, centric-ordered, segmented, refocused 3D-SSFP sequence was used in combination with Real-time Motion Correction (RMC), which detects the position of the diaphragm with crossed probing pulses for prospective real-time gating (gating window 4.65 mm) and performs volume tracking (motion correction factor 0.6) based on the one-dimensional data of the right diaphragm position [14]. For cardiac synchronization and monitoring, two electrodes were placed on the left anterior hemithorax of the subject and the R wave of the electrocardiogram was used as a trigger for image acquisition with a certain time delay. The magnetization was prepared by a T2-preparation pulse, followed by a frequency-selective fat saturation pulse and a spoiler gradient [15]. Scanning was performed with parameters of TR 4.3 ms, TE 2.2 ms, FA 120°, in in-plane readout and phase encodings of 256 × 192, resulting in a resolution of 1.3 and 1.5 mm, respectively. Eighty transverse slices of 1.5 mm thickness were acquired to cover the entire heart. The image was reconstructed to the voxel size of 0.6 × 0.6 × 0.75 mm. Scan acceleration was applied in both phase- and slice-encoding directions with the factors of 2 and 1.5, respectively. The acquisition window was divided into 4 segments of 98.7 ms. For each acquisition, the scan time was limited to 20 min and the scan was aborted when the scan time was over this limit.

Visual feedbacks

The breathing level measured by RMC, was converted to a video signal, projected onto a screen in front of the scanner by an LCD projector (CP-SX1350, Hitachi, Tokyo, Japan) outside of the scan room and viewed by the patient though an inner-bore mirror, so that subjects could adjust their breathing level.

The WH-CMRA was acquired under three conditions: (1) free breathing without VFB (FB − VFB),

i.e. a conventional method, (2) free breathing with VFB (FB + VFB) and (3) multiple breath-hold with VFB (MBH + VFB). The subjects were instructed to take steady and small breaths in the FB − VFB condition, and to adjust the end-expiration point within the gating window of 4.65 mm in the RMC + VFB condition. In the MBH + VFB condition, subjects were instructed to expire slowly and hold breath when the position of the diaphragm came into the gating window and keep it while they do not feel a need to breath, for approximately 5–10 s. The first scan condition was fixed to FB − VFB, where the scan was conducted without any special instruction. In the second and third scans, conditions of FB + VFB and MBH + VFB were used in an alternative order for successive subjects in order to avoid a learning effect.

Image processing

The data from 3D CMRA was transferred to a commercially available workstation with image reconstruction software (AZE Virtual Place, AZE Ltd, Tokyo, Japan). For each of the RCA, left anterior descending (LAD), and left circumflex (LCX), multiple contiguous sections were selected and curved multiplanar reconstruction (CPR) images were created by a radiological technologist.

Assessment of image quality

Assessment of 3D CMRA quality was conducted by two readers (T.O. and S.K.) in consensus. The information on subject and scan conditions was made blind to these readers. The coronary segments were classified using the system described by the American Heart Association: RCA was divided into segments 1–4, LAD was divided into segments 5–10 and LCX was divided into segments 11–15. In order to grade the image quality of all the coronary artery segments, a five-point grading system was used: (4) excellent (the vessel was well depicted with sharply defined borders), (3) fair (the vessel was adequately visualized, with confidence in the diagnosis, only mildly blurred borders), (2) good (coronary vessel was visible, but confidence in the diagnosis was low, due to moderately blurred borders), (1) poor (coronary vessel barely seen, or was obscured by noise), and (0) not visualized [16, 17]. For the evaluation, both the original and CPR images were used.

Statistical analysis

Comparisons were made by means of paired *t*-test for continuous variables and Mann–Whitney test for nominal variables. In all cases, a two-tailed test was performed. *P* values of 0.05 or less were considered statistically significant.

Results

Subject characteristics

Of 13 subjects, 2 (15%) could not complete the scan within the 20 min limit without VFB, and they were excluded from further analysis. The average heart rate of the subjects was 59 beats per minute, ranging from 49 to 74, and the acquisition was performed at the stationary period in diastolic phase [17]. The mean stationary period of RCA was 246 ms, varying from 112 to 368 ms. The length of the acquisition window was 98.7 ms and the whole scan was performed within the cardiac rest period. Representative breathing patterns for different scan conditions are presented in Fig. 1.

Scan time

The average scan time (mean ± SD) was 10.0 ± 2.2, 10.0 ± 2.5 and 8.2 ± 1.3 min for FB − VFB, FB + VFB, and MBH + VFB, respectively (Fig. 2). The MBH scan with VFB had significantly reduced scan time by 18% compared with both FB scans ($P < 0.05$). The average scan times were almost identical for FB scans with and without VFB, due to four cases (36%) having rather longer scan times with VFB than without it. The FB − VFB scan was not completed within 20 min in two subjects due to changes in breathing level, but other scans were completed within this time limit. Hence, the substantial difference was larger, if these failed examinations were taken into consideration.

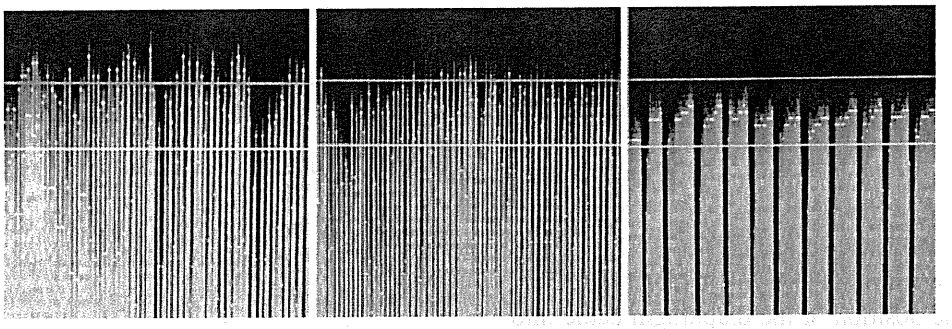

Fig. 1 Representative breathing patterns for different scan methods. Free-breathing without visual feedback (FB − VFB) (*left*), free-breathing with visual feedback (FB + VFB) (*center*), multiple breath-hold with visual feedback (MBH + VFB) (*right*). *Two horizontal bars* indicate the gating window of 4.65 mm and *small dots* indicate diaphragm positions. Better fit into the gating window was observed in scans with VFB

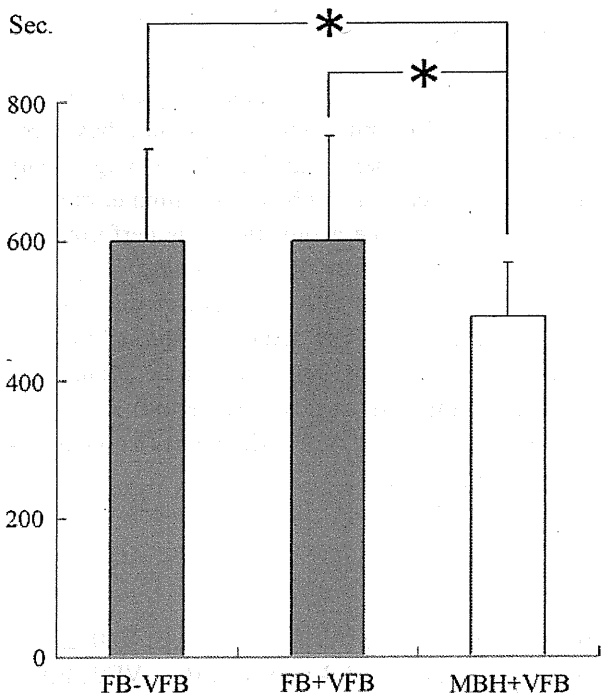

Fig. 2 Average acquisition times for different scan methods. Acquisition time was significantly reduced in MBH + VFB compared with FB with or without VFB. * $P < 0.05$

Image quality evaluation

There were no significant differences in average scores between FB − VFB and MBH + VFB ($P > 0.05$, Fig. 3). Significant score reductions ($P < 0.05$) were observed for FB + VFB at 5 segments (#1, 2, 5, 7, 11) and 7 segments (#1, 2, 3, 4, 5, 7, 11) in comparison with FB − VFB and MBH + VFB, respectively (Table 1). However, two subjects had equal or better average scores of 2.0 and 1.9 in FB + VFB compared with the other scan conditions (average scores equal or less than 1.9).

Discussion

Free-breathing coronary artery scan gated with diaphragm position [18] typically use probing pulses positioned through the dome of the right hemidiaphragm and an acceptance window of 5 mm to give a reasonable compromise between scan efficiency and image quality. However, during prolonged studies, such as WH-CMRA, drifting of the respiratory pattern leads to a corresponding fall in efficiency [6], resulting in registration errors between scans and a frequent need to reposition the acceptance window. Alternatively, WH-CMRA can be performed during multiple breath-holds, but, patients cannot hold their breath for the same amount of time and misregistration of the diaphragm between breath-holds is responsible for poor image quality with the conventional breath-hold CMRA technique [3]. Motion of the coronary artery is caused by respiration and leads to image blurring and the creation of ghost artifacts [4, 19, 20]. To overcome these problems, a feedback system of respiration level would be beneficial. In the scan condition without feedback of breathing level, 2 of 13 subjects could not complete the scan within 20 min, while all subjects were able to complete the scan in the other conditions with VFB, illustrating the effectiveness of this system for successful WH-CMRA.

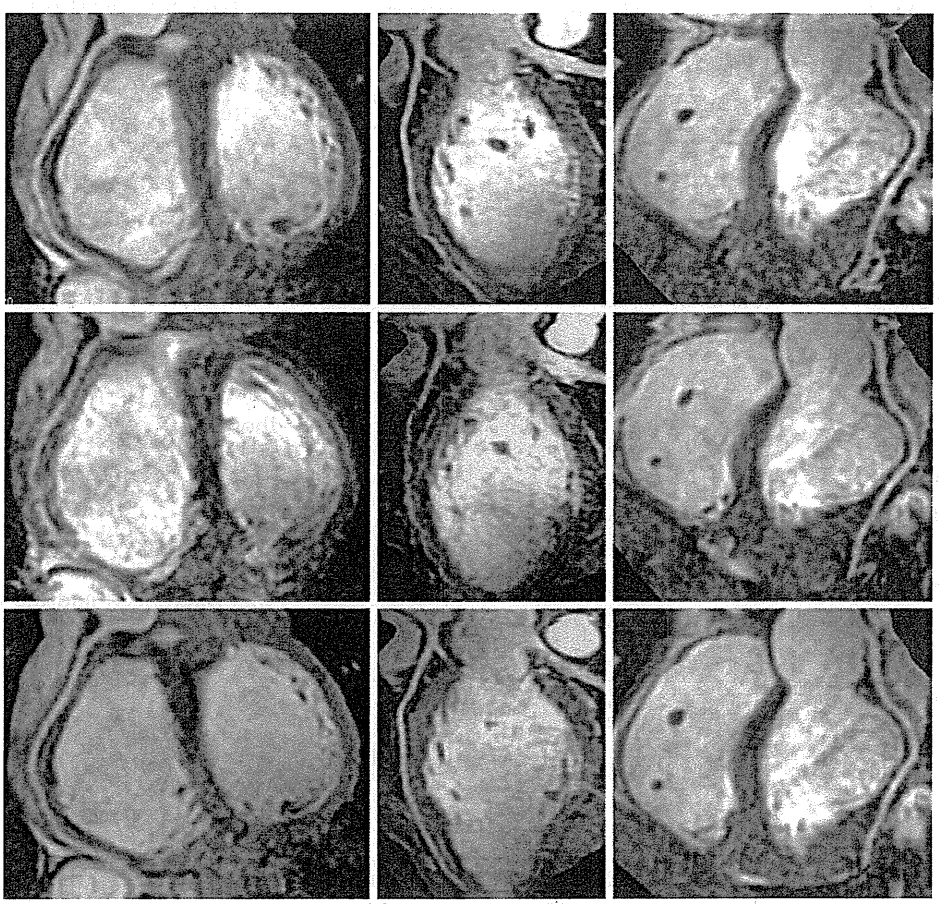

Fig. 3 Representative coronary artery images with different scan methods. Images of RCA (*left*), LAD (*center*) and LCX (*right*) are presented for FB − VFB (*top*), FB + VFB (*middle*) and MBH + VFB (*bottom*). Images of similar quality are obtained for FB − VFB and MBH + VFB. Image quality of the FB + VFB condition is slightly degraded. *RCA* right coronary artery, *LAD* left anterior descending, *LCX* left circumflex

There were two possible methods to adjust the depth of breath, free-breathing and multiple breath-holds. By using the MBH + VFB method, the scan time was significantly reduced (on average by 18%), while the visualization quality of the coronary arteries was the same as that of the no feedback condition. In this method, data was acquired during the readout period that was less affected by respiratory motion, but no significant difference in image quality was observed. According to debriefing after the scan, subjects were able to perform better, because they could slowly adjust the breathing level in the initial few feedbacks and kept the breath-hold position after it occurred within the gating window in the MBH + VFB method. Longer breath-hold may have further reduced scan time, but the breath-hold was limited to approximately 5–10 s, because breath-holding for a long duration is known to cause large diaphragm displacement and heart rate change [5].

In contrast, the average scan times were almost identical for FB scans with and without VFB and was due to four cases (36%) having longer scan time with VFB than without it. The result could be due to the long time constant and infrequency of the feedback (once per heart beat). Subjects had difficulty in controlling the depth of each breath under such conditions resulting in significant reduction in the image quality at some coronary segments. However, two subjects showed equal to or better than average quality scores in FB + VFB than the other scan conditions and were considered to be able to control breathing level with high precision. Hence some subjects are suitable for the FB + VFB, but their numbers might be limited. For application to more subjects, the feedback time constant must be shortened and more frequent updates on diaphragm position should be presented.

A potential drawback of the proposed methods is the need for patient cooperation. Clinical trials of the VFB system have to be conducted to determine the significance of this limitation. Multiple breath-hold scans with VFB would be the first choice among the

Table 1 Image quality scores of coronary artery segments

Coronary artery segments	Image quality scores (mean ± SD)		
	FB − VFB	FB + VFB	MBH + VFB
#1	3.5 ± 0.7	2.9 ± 0.5*1,2	3.3 ± 0.6
#2	3.4 ± 0.5	2.9 ± 0.3*1,2	3.4 ± 0.5
#3	2.6 ± 0.8	2.4 ± 0.7*2	2.9 ± 0.9
#4	1.4 ± 0.8	1.2 ± 0.9*2	1.7 ± 1.0
#5	3.0 ± 0.6	2.5 ± 0.7*1,2	2.9 ± 0.5
#6	2.5 ± 0.5	2.5 ± 0.7	2.6 ± 0.5
#7	2.5 ± 0.5	1.8 ± 0.9*1,2	2.2 ± 0.8
#8	0.6 ± 0.5	0.7 ± 0.5	0.6 ± 0.5
#9	1.6 ± 0.7	1.3 ± 0.8	1.3 ± 0.5
#10	0.6 ± 0.8	0.5 ± 0.7	0.4 ± 0.7
#11	2.7 ± 0.5	2.2 ± 0.8*1,2	2.6 ± 0.7
#12	1.7 ± 0.8	1.3 ± 0.6	1.6 ± 0.7
#13	1.9 ± 0.5	1.6 ± 0.8	1.9 ± 0.7
#14	1.1 ± 0.7	0.8 ± 0.6	0.9 ± 0.7
#15	0.1 ± 0.3	0.1 ± 0.3	0.1 ± 0.3

Significantly worse scores were observed in FB + VFB than FB − VFB*1 and MBH + VFB*2 ($P < 0.05$). There was no significant difference between FB − VFB and MBH + VFB

scan methods due to significantly shorter scan times without loss of image quality. However, repetitive breath-holds have a potential to be a problem for patient examination. When 50 patients were studied for their repetitive breath-holding capabilities, the 95% confidence interval for the average numbers of 12 s breath holds was 4.9 for patients of chronic obstructive pulmonary disease and 6.6 for patients of congestive heart failure [21]. For the multiple breath-hold scan with VFB, subjects were instructed to maintain the breath-hold within approximately 5–10 s so that they would not feel a need to breathe and higher numbers of multiple breath-holds would be possible. The MBH + VFB method would be acceptable even for patients and contribute to more efficient scans of the coronary artery.

In this study, estimation of coronary rest period was visually assessed on the RCA in a single plane of 4-chamber view. Assessment of coronary motion in a single imaging plane has been shown to be limited because the 3D movement of the vessels—in particular, motion through the imaging plane and the motion at different levels of the vessel—cannot be completely assessed [22], although visual evaluation of movement for the entire heart is not feasible. Undetected motion of LCA might result in a slight increase in the number of motion artifact, which was observed as decreased scores. The duration of the cardiac rest period was reported to be shorter for the RCA compared with the LAD and the onset of the rest period was more delayed for the RCA in the averaged data of 15 subjects [23]. However, in a CMRA study of 210 consecutive patients, Jahnke et al. observed that in about one-third of patients, the rest period of LCA began later or was shorter than that of RCA [24], possibly explaining the inferior image quality scores of LCA segments than those of RCA segments.

There are several limitations in this study. It included only a limited number of healthy volunteers and no patient was included. Therefore, no gold standard, such as findings of invasive angiography was referenced and the proposed methods need to be validated in a patient population, including quantitative evaluation of stenosis severity.

Acknowledgments This study was conducted as a part of the project, "R&D of Molecular Imaging Equipment for Malignant Tumor Therapy Support," supported by NEDO (New Energy and Industrial Technology Development Organization), Japan.

References

1. Frahm J, Haase A, Matthaei D (1986) Rapid three-dimensional MR imaging using the FLASH technique. J Comput Assist Tomogr 10:363–368. doi:10.1097/00004728-198603000-00046
2. Parker DL, Gullberg GT (1990) Signal-to-noise efficiency in magnetic resonance imaging. Med Phys 17:250–257. doi:10.1118/1.596503
3. Taylor AM, Keegan J, Jhooti P et al (1999) Differences between normal subjects and patients with coronary artery disease for three different MR coronary angiography respiratory suppression techniques. J Magn Reson Imaging 9:786–793. doi:10.1002/(SICI)1522-2586(199906)9:6<786::AID-JMRI5>3.0.CO;2-T
4. Wang Y, Grist TM, Korosec FR et al (1995) Respiratory blur in 3D coronary MR imaging. Magn Reson Med 33:541–548. doi:10.1002/mrm.1910330413
5. Holland AE, Goldfarb JW, Edelman RR (1998) Diaphragmatic and cardiac motion during suspended breathing: preliminary experience and implications for breath-hold MR imaging. Radiology 209:483–489
6. Taylor AM, Jhooti P, Wiesmann F et al (1997) MR navigator-echo monitoring of temporal changes in diaphragm position: implications for MR coronary angiography. J Magn Reson Imaging 7:629–636. doi:10.1002/jmri.1880070404

7. Korin HW, Ehman RL, Riederer SJ et al (1992) Respiratory kinematics of the upper abdominal organs: a quantitative study. Magn Reson Med 23:172–178. doi:10.1002/mrm.1910230118
8. Liu YL, Riederer SJ, Rossman PJ et al (1993) A monitoring, feedback, and triggering system for reproducible breath-hold MR imaging. Magn Reson Med 30:507–511. doi:10.1002/mrm.1910300416
9. Wang Y, Grimm RC, Rossman PJ et al (1995) 3D coronary MR angiography in multiple breath-holds using a respiratory feedback monitor. Magn Reson Med 34:11–16. doi:10.1002/mrm.1910340104
10. Foo TK, Saranathan M, Hardy CJ et al (2000) Coronary artery magnetic resonance imaging: a patient-tailored approach. Top Magn Reson Imaging 11:406–416. doi:10.1097/00002142-200012000-00009
11. Pruessmann KP, Weiger M, Scheidegger MB et al (1999) SENSE: sensitivity encoding for fast MRI. Magn Reson Med 42:952–962. doi:10.1002/(SICI)1522-2594(199911)42:5<952::AID-MRM16>3.0.CO;2-S
12. Weiger M, Pruessmann KP, Boesiger P (2002) 2D SENSE for faster 3D MRI. MAGMA 14:10–19. doi:10.1007/BF02668182
13. Weber OM, Martin AJ, Higgins CB (2003) Whole-heart steady-state free precession coronary artery magnetic resonance angiography. Magn Reson Med 50:1223–1228. doi:10.1002/mrm.10653
14. Danias PG, McConnell MV, Khasgiwala VC et al (1997) Prospective navigator correction of image position for coronary MR angiography. Radiology 203:733–736
15. Botnar RM, Stuber M, Danias PG et al (1999) Improved coronary artery definition with T2-weighted, free-breathing, three-dimensional coronary MRA. Circulation 99:3139–3148
16. Sakuma H, Ichikawa Y, Suzawa N et al (2005) Assessment of coronary arteries with total study time of less than 30 minutes by using whole-heart coronary MR angiography. Radiology 237:316–321. doi:10.1148/radiol.2371040830
17. Wu YW, Tadamura E, Yamamuro M et al (2007) Evaluation of three-dimensional navigator-gated whole heart MR coronary angiography: the importance of systolic imaging in subjects with high heart rates. Eur J Radiol 61:91–96. doi:10.1016/j.ejrad.2006.08.013
18. Oshinski JN, Hofland L, Mukundan S et al (1996) Two-dimensional coronary MR angiography without breath holding. Radiology 201:737–743
19. Schultz CL, Alfidi RJ, Nelson AD et al (1984) The effect of motion on two-dimensional Fourier transformation magnetic resonance images. Radiology 152:117–121
20. Wood ML, Henkelman RM (1986) Suppression of respiratory motion artifacts in magnetic resonance imaging. Med Phys 13:794–805. doi:10.1118/1.595851
21. Gay SB, Sistrom CL, Holder CA et al (1994) Breath-holding capability of adults. Implications for spiral computed tomography, fast-acquisition magnetic resonance imaging, and angiography. Invest Radiol 29:848–851. doi:10.1097/00004424-199409000-00009
22. Hofman MB, Wickline SA, Lorenz CH (1998) Quantification of in-plane motion of the coronary arteries during the cardiac cycle: implications for acquisition window duration for MR flow quantification. J Magn Reson Imaging 8:568–576. doi:10.1002/jmri.1880080309
23. Kim WY, Stuber M, Kissinger KV et al (2001) Impact of bulk cardiac motion on right coronary MR angiography and vessel wall imaging. J Magn Reson Imaging 14:383–390. doi:10.1002/jmri.1198
24. Jahnke C, Paetsch I, Achenbach S et al (2006) Coronary MR imaging: breath-hold capability and patterns, coronary artery rest periods, and beta-blocker use. Radiology 239:71–78. doi:10.1148/radiol.2383042019

Uterine Peristalsis in Women With Repeated IVF Failures: Possible Therapeutic Effect of Hyoscine Bromide

Aki Kido, MD, PhD,[1] Kaori Togashi, MD, PhD,[1] Hiroshi Hatayama, MD, PhD,[2] Takahiro Nakayama, MD, PhD,[2] Akira Yamamoto, MD, PhD,[1] Masako Kataoka, MD, PhD, MPhil,[1] Togas Tulandi, MD, MHCM[3]

[1]Department of Diagnostic Imaging and Nuclear Medicine, Kyoto University, Kyoto City, Kyoto, Japan

[2]Adachi Hospital, Kyoto, Kyoto, Japan

[3]Department of Obstetrics and Gynecology, McGill University, Montreal QC

Abstract

Background: Uterine peristalsis, which is influenced by hormonal and cholinergic effects, may have a role in successful implantation and continuing pregnancy.

Cases: We encountered abnormal uterine peristalsis in three women who had had repeated in vitro fertilization (IVF) treatment failures. They subsequently had successful pregnancies when hyoscine bromide was administered at the time of embryo transfer.

Conclusion: It is possible that decreasing uterine peristalsis with use of an anticholinergic agent during IVF treatment facilitates retention of embryos and increases the probability of successful pregnancy.

Résumé

Contexte : Le péristaltisme utérin, lequel est influencé par des effets hormonaux et cholinergiques, pourrait jouer un rôle dans la réussite de l'implantation et de la poursuite de la grossesse.

Cas : Nous avons constaté un péristaltisme utérin anormal chez trois femmes qui avaient subi des échecs à répétition dans le cadre d'un traitement de fécondation *in vitro* (FIV). Elles ont par la suite connu une grossesse réussie lorsqu'on leur a administré du bromure d'hyoscine au moment du transfert d'embryon.

Conclusion : Il est possible que l'atténuation du péristaltisme utérin au moyen d'un agent anticholinergique au cours du traitement de FIV facilite la rétention des embryons et entraîne la hausse de la probabilité de réussite de la grossesse.

J Obstet Gynaecol Can 2009;31(8):732–735

Key Words: infertility, MRI, uterine peristalsis, anti-cholinergic agent, hyoscine

Competing Interests: None declared.

Received on February 10, 2009

Accepted on March 10, 2009

INTRODUCTION

Uterine peristalsis may play a role in the ability to conceive[1–6]; unusual patterns of peristalsis have been observed in women with endometriosis and infertility.[7,8] Uterine peristalsis is under the influence of hormones,[9] and its activity can be suppressed by anticholinergic agents.[10] We report the identification of unusual uterine peristalsis in three infertile women who subsequently had successful pregnancies with in vitro fertilization (IVF) treatment combined with administration of an anticholinergic agent.

THE CASES

Case One

A 30-year-old woman had a six-year history of unexplained infertility. She had previously undergone six cycles of IVF and multiple embryo transfers without success. In the first IVF cycle, three embryos (two 8-cell and one 4-cell, all of good quality) were transferred. Pregnancy did not occur, and in the subsequent cycle three frozen-thawed embryos (two 5-cell and one 4-cell embryo, of good to medium quality) were transferred. Again, pregnancy did not occur, and in the next IVF cycle a two-step consecutive transfer of a frozen-thawed embryo (4-cell good quality) and two blastocysts was performed.

Subsequently, we transferred two frozen-thawed embryos (5-cell good quality and 5-cell poor quality) but without success. Sperm concentration and sperm quality were normal in all treatment cycles. Four additional cycles of IVF with blastocyst transfer also failed.

After obtaining written informed consent, we performed a uterine peristalsis study as previously described.[11–13] As

A serial image taken from 60 HASTE images in Case 2. Thickest and/or darkest areas within the junctional zone are indicated by arrows. These areas move from fundus to cervix with distortion of the endometrial configuration. (a) Thickest area of junctional zone at the fundus. The endometrial outline is made concave by contraction at the fundus. (b) Darkest area of junctional zone has moved to the middle of the uterine corpus. The endometrial cavity is compressed at those points. (c) Thickest and darkest areas within the junctional zone have moved to the uterine cervix.

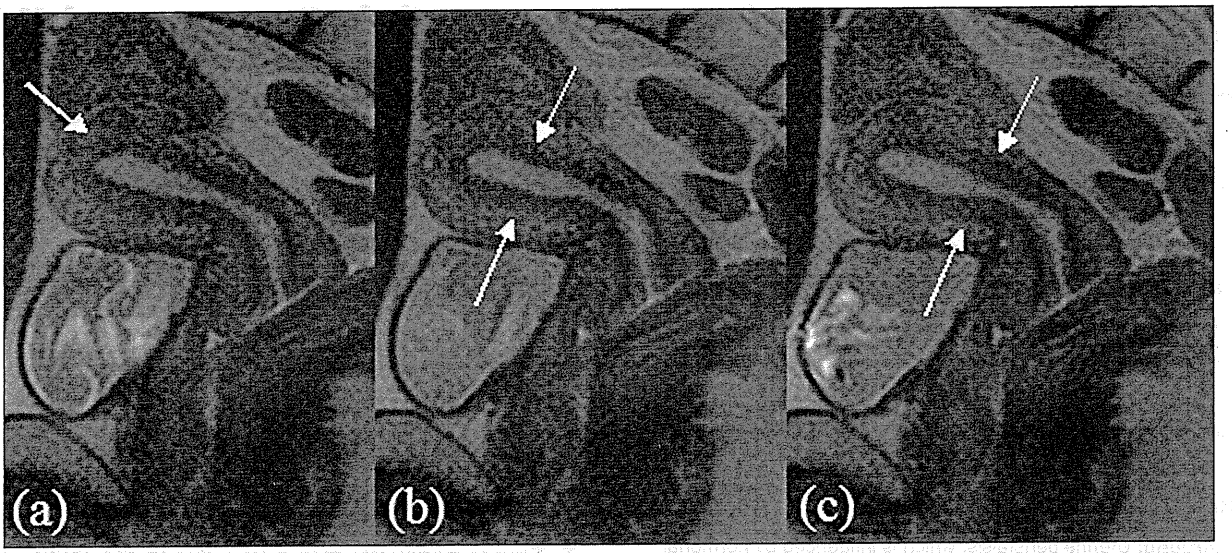

usual, it was performed in the late follicular phase of a natural cycle when the dominant follicle was ≥ 18 mm in diameter. The study consisted of acquisition of cine MR images using a 1.5-T magnet unit (Symphony; Siemens Medical Systems, Erlangen, Germany) every three seconds over three minutes, and repeated after five minutes. The images were analyzed using an original computer assisted program.[14]

The first cine MRI was performed on day 13 of a 27-day cycle, and we identified peristaltic waves passing from the fundus to the cervix seven times in three minutes. In the second scan, the number of peristaltic waves was the same, but the direction was mixed (cervical–fundal and fundal–cervical). We administered hyoscine butylbromide 20 mg intramuscularly (Buscopan, Nippon Boehringer Ingelheim, Hyogo, Japan), and the uterine peristalsis study was repeated five minutes later. On this occasion, peristalsis was identified four times in three minutes, with fundal–cervical direction.

Subsequently, the patient underwent another IVF treatment with injection of hyoscine butylbromide prior to embryo transfer. We transferred two 8-cell embryos of good quality and two blastocysts. The patient conceived, but unfortunately the pregnancy was ectopic, and she underwent a right salpingectomy. A year later, she underwent another IVF treatment cycle and had a frozen-thawed blastocyst transfer with hyoscine injection just before transfer. The patient conceived with an intrauterine pregnancy and subsequently delivered a healthy boy weighing 2900 g.

Case Two

This 34-year-old woman had an eight-year history of unexplained infertility and had undergone four failed IVF treatment cycles elsewhere.

We performed a uterine peristalsis study. The first preovulatory MR scan on cycle day 12 of a 29-day cycle identified uterine peristalsis six times in three minutes, and in the second scan it was identified eight times in three minutes. The direction of peristalsis was fundal-cervical on both occasions (Figure). In a subsequent IVF treatment cycle with hyoscine injection, we transferred two high-quality 4-cell embryos. An intrauterine pregnancy was achieved, but the patient subsequently miscarried. In a subsequent IVF cycle with hyoscine administration, two high-quality 4-cell embryos were transferred, resulting in pregnancy and subsequent delivery of a healthy girl weighing 3152 g.

Case Three

This 33-year-old woman had a five-year history of unexplained infertility, with several failed IVF treatment cycles. In the first and second IVF cycles, we had transferred one good quality 8-cell embryo, and three smaller embryos (a 4-cell, a 3-cell, and a 2-cell) respectively. In the next treatment cycle, three frozen-thawed embryos (one 6-cell, and two 4-cell) were transferred, and in the cycle after that two

frozen-thawed embryos (both 6-cell) were transferred without success.

The uterine peristalsis study done on day 15 of a 30-day cycle showed fundal–cervical waves two times in three minutes during the first and second MR scans. In the subsequent IVF treatment cycle, with hyoscine administration, a two-step embryo transfer (a 5-cell embryo and a 3-cell embryo, followed two days later by a blastocyst) was performed. The patient conceived and subsequently delivered a healthy boy weighing 3620 g.

DISCUSSION

Our cine MR studies demonstrated that the direction of uterine peristalsis in the follicular phase is from fundus to cervix, with a frequency of two to six times in three minutes. In the periovulatory phase, it propagates in the opposite direction, from cervix to fundus, with a frequency of 3.5 ± 0.6 times per minute.[3,15–18] In the luteal phase, the frequency of peristalsis decreases, relaxing the uterus.[3,15–17]

Ijland et al. reported that periovulatory fundal–cervical peristalsis was most frequently observed in women who never conceived.[1] They also found active uterine peristalsis in the mid-luteal phase among 46% of women who never conceived compared with 11% in those who subsequently conceived.[1]

We studied uterine peristalsis in three women with long-standing unexplained infertility and repeated IVF failures. In contrast to the usual periovulatory cervical–fundal direction of uterine peristalsis, these women had had peristaltic waves in the opposite direction. Fundal–cervical waves may impair sperm transport, and expel an embryo from the uterine cavity. Administration of hyoscine bromide in the patient described in Case 1 decreased the frequency of uterine peristalsis, mitigating these deleterious effects. Pierzynski et al. reported that administration of an oxytocin antagonist also decreased uterine contractility.[19] As a result, the embryo is retained in the uterine cavity. Franchin et al. found that a low frequency of peristaltic waves at the time of embryo transfer was related to successful implantation and pregnancy.[5]

Hyoscine is an anticholinergic drug that is well absorbed after oral or parenteral administration. Animal studies have shown that it is not teratogenic (unpublished data, Nippon Boehringer Ingelheim). The duration of effect is about 40 minutes after an intramuscular injection, but its metabolites remain in the body for a few hours.[20]

Administration of hyoscine in our patients appeared to be beneficial. It suggests a possible role of this agent in the treatment of infertility. A randomized controlled trial to evaluate the efficacy of hyoscine on the pregnancy rate is clearly needed.

Our report has some limitations. Although previous reports have shown the effects of estradiol, oxytocin, progesterone, and other substances on uterine contractility,[21–23] we did not assess hormone concentrations. We did not conduct the uterine peristalsis studies at the time of embryo transfer, which may have shown a different pattern from the study done in the late preovulatory phase. In addition, we do not have information about the reproducibility of uterine peristaltic studies. Finally, subtle differences in embryo quality might have accounted for the different outcomes of IVF treatment with and without hyoscine treatment.

CONCLUSION

This preliminary report suggests that women with repeated IVF failures might have abnormal uterine peristalsis. It is possible that decreasing peristalsis by administration of hyoscine increases the chance of embryo retention, implantation, and successful pregnancy. Further study in a large number of patients is needed.

ACKNOWLEDGMENTS

The women whose stories are told in this report have provided written consent for its publication.

The study was conducted at and supported by Department of Diagnostic Imaging and Nuclear Medicine, Graduate School of Medicine, Kyoto University, Kyoto City, Kyoto, Japan.

The authors express their appreciation to Dr Caroline Reinhold, MD (Department of Diagnostic Radiology, McGill University Health Centre, Montreal, Quebec) for assistance with preparation of the manuscript, and to Dr Naoki Asada, PhD (Department of Intelligent Systems, Hiroshima City University, Hiroshima, Japan), Mr Masahide Nishiura (Corporate Research & Development Center, Toshiba Corporation, Japan), Dr Asako Nakai, MD, PhD (Department of Diagnostic Imaging and Nuclear Medicine, Kyoto University, Japan), and Dr Koji Fujimoto, MD (Department of Diagnostic Imaging and Nuclear Medicine, Kyoto University, Japan) for excellent technical assistance and for proofreading the manuscript.

REFERENCES

1. Ijland MM, Evers JL, Dunselman GA, Volovics L, Hoogland HJ. Relation between endometrial wavelike activity and fecundability in spontaneous cycles. Fertil Steril 1997;67:492–6.

2. Ijland MM, Hoogland HJ, Dunselman GA, Lo CR, Evers JL. Endometrial wave direction switch and the outcome of in vitro fertilization. Fertil Steril 1999;71:476–81.

3. Kunz G, Beil D, Deininger H, Wildt L, Leyendecker G. The dynamics of rapid sperm transport through the female genital tract: evidence from